# Localized traveling waves in vertical-cavity surface-emitting lasers with frequency-selective optical feedback

P. V. Paulau,[1,2] A. J. Scroggie,[2] A. Naumenko,[1] T. Ackemann,[2] N. A. Loiko,[1] and W. J. Firth[2]
[1]*Institute of Physics, NASB, Belarus, Scaryna Prospekt 70, 220072 Minsk*
[2]*Department of Physics, University of Strathclyde, 107 Rottenrow East, Glasgow G4 0NG, United Kingdom*
(Received 5 September 2006; revised manuscript received 18 December 2006; published 17 May 2007)

Spatially self-localized states have been found in a model of vertical-cavity surface-emitting lasers with frequency-selective optical feedback. The structures obtained differ from most known dissipative solitons in optics in that they are localized traveling waves. The results suggest a route to realization of a cavity soliton laser using standard semiconductor laser designs.

DOI: 10.1103/PhysRevE.75.056208 PACS number(s): 42.65.Tg, 42.81.Dp

## I. INTRODUCTION

Localized structures or solitary wave packets have been found in numerous dissipative nonequilibrium systems of different natures and have attracted a lot of interest in recent years (see, e.g., [1,2] for reviews). Nonlinear optical systems, where they are often referred to as *cavity solitons*, present attractive opportunities to investigate the properties of such localized structures (see, e.g., [2–10]). Moreover, due to their bistable nature and motility these structures may find practical implementation for communication technologies and information processing, especially if realized in fast and compact devices such as semiconductor microcavities [7].

In most nonlinear optical systems where cavity solitons have been investigated, they are sustained against losses by an injected holding beam of high spatial and temporal coherence [3,7,11,12]. This has several disadvantages for applications. Here we investigate a system which requires no holding beam, namely, a vertical-cavity surface-emitting laser (VCSEL) with frequency-selective feedback (FSF) from an external grating. In such a "cavity soliton laser" [4,6,13] the emission could be completely sustained by means of a simple and inexpensive incoherent pumping mechanism, namely, current injection. Optical bistability (OB) between the off state and the lasing external cavity mode has been found in such a system, but with a small-area VCSEL [14,15]. OB is often an indicator that pattern formation and localized states can be found in an analogous broad-area device, where transverse degrees of freedom come into play.

Broad-area VCSELs, when the peak gain is blue detuned from the longitudinal cavity resonance, exhibit tilted-wave emission [16], in which the transverse component of the wave vector compensates for the detuning. Typically, several (or many) tilted waves are excited, and the spatial structure of the laser emission is usually quite complex. Channeling the emission into a single tilted wave, with a soliton-type envelope, would be attractive for applications. Our approach to this goal is based on using an external cavity to provide the necessary frequency and wave vector selectivity.

In the present work we develop a model of a broad-area VCSEL with FSF and demonstrate that it supports grating-controlled transverse traveling-wave modes. We find a parameter range in which such modes coexist with a stable trivial solution (laser "off"), which is a necessary condition for soliton existence. Numerical simulations, however, typically show complex dynamics, because a large number of tilted waves can be excited and compete with each other. We therefore introduce an annular spatial filter into the feedback path. We then find winner-take-all competition between the tilted waves on the annulus, leading asymptotically to a single dominant transverse traveling wave. We next show that this system does indeed support cavity solitons in the form of localized traveling waves (LTWs) on a stable dark (nonlasing) background. These LTWs are stable over long integration times, and pass standard tests for dissipative solitons, such as exponential decay in the transverse direction (i.e., boundary independence). Further, several LTWs can exist at different transverse locations, with no significant interaction (if the distances between them are sufficiently large), perhaps the most desirable property of a cavity soliton laser [6,13]. Because of azimuthal symmetry, these LTWs form a whole family, with different orientations. In addition, we find a cylindrically symmetric localized structure, which we term a localized standing wave.

Compared to other approaches to a cavity soliton laser (see, e.g., [4,6] for nonsemiconductor materials and [17] for a proposed semiconductor-based device) relying on the integration of a gain medium and a saturable absorber within the cavity, our approach has the attractive feature that it can be implemented using standard VCSEL structures and off-the-shelf optical components.

The paper is organized as follows. We begin by describing the VCSEL FSF system, and formulate a set of delay-differential equations to describe its spatiotemporal behavior. Initially considering the case of a flat (or very broad) gain spectrum, we solve these equations analytically for transverse traveling-wave solutions. For on-axis modes, we demonstrate how FSF introduces a band of grating-controlled modes with current thresholds below, and split off from, those of the solitary laser, with bistability between lasing and nonlasing states for current values in the gap. Next, we show that off-axis traveling-wave modes usually close this gap, but that phase-amplitude coupling allows it to reopen for appropriate detuning between the grating and cavity resonances. We then introduce spatial filtering to limit the wave vector spectrum, and also take account of finite gain bandwidth. We next present numerical results for this final model: the emergence from noise of a single dominant traveling-wave mode,

 

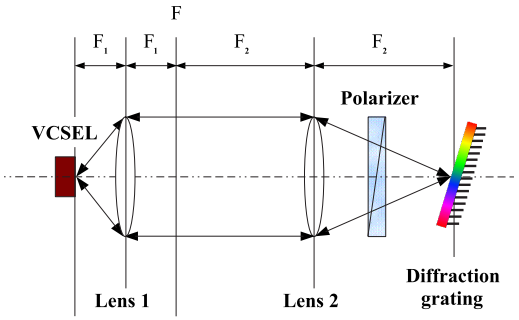


FIG. 1. (Color online) The scheme of the system. $F_1$ is the focal length of the first lens, and $F_2$ that of the second lens.

and then of a stable LTW from an initial condition comprising a finite disk of this dominant mode. Results of several tests follow, showing that this LTW is solitonic. We conclude with a summary of our results, and a discussion of the experimental and applications prospects of this interesting type of cavity soliton.

## II. SYSTEM AND MODEL

The scheme of the proposed system is depicted in Fig. 1, where a VCSEL is coupled to an external cavity formed by an afocal telescope and closed by a diffraction grating. Due to the self-imaging configuration, effectively no diffraction takes place in the external cavity. For one particular frequency, which can be adjusted by turning the grating, the grating behaves as a normal mirror and closed paths exist for all wave vectors after one round trip in the external cavity. For a wave detuned from this frequency, rays still arrive at the original position but at a different angle, i.e., with a reduced amplitude at the original transverse wave vector. The shifted components are rejected by the VCSEL cavity due to the angular selectivity of the resonance. The grating thus provides a frequency filtering mechanism (with a sinc-shaped spectrum). Evidence for frequency selection was found in an experimental configuration similar to that of Fig. 1 [18] (see also [15]). For simplicity, we are going to assume here that the feedback efficiency is the same for all wave vectors and depends only on the frequency detuning. The results are not expected to be sensitive to the profile of the filter function in frequency space as long as it is a well-behaved single-hump function, and similar results can be expected in other configurations with frequency-filtered feedback [19].

Several models have been used to analyze spatial structure in free-running VCSELs [20–23]. For the purpose of describing spontaneous pattern formation in broad-area devices, that used in Ref. [21] is particularly well suited, and is the basis of the model used here. The dynamics of a VCSEL should in general be described by vectorial equations [24]. However, we will study the case of strongly anisotropic feedback, where the $y$ component of the field is absorbed and feedback exists only for the $x$ component. Moreover, the system is operated below the threshold of the solitary VCSEL, and hence only $x$-polarized emission can be excited.

We write the $x$ component of the intracavity optical field as $\mathcal{E}_x = E\exp(i\omega_c t) + \text{c.c.}$, where $\omega_c$ is a reference frequency, chosen to be that of the longitudinal cavity resonance at threshold. Our model is then based on an equation for the slowly varying amplitude $E$, coupled to a real equation for the carrier inversion density $N$:

$$\frac{\partial E}{\partial t} = -\kappa(1+i\alpha)E + \kappa(1+i\alpha)N\hat{\mathcal{L}}E - ia\Delta_\perp E + F,$$

$$\frac{\partial N}{\partial t} = -N + \mu - NE^*\hat{\mathcal{L}}E. \tag{1}$$

The variable $N$ is normalized such that $N=0$ at transparency, and $N=1$ at the threshold of the solitary VCSEL, at which the normalized injection current $\mu=1$. Time is normalized to the carrier relaxation time (expected to be around 1 ns) and $\kappa \gg 1$ is the mean decay rate of the field in the cavity. $\alpha$ is the linewidth enhancement factor describing phase-amplitude coupling, and the operator $\hat{\mathcal{L}}$ describes the gain spectrum, assumed Lorentzian in frequency space, $\hat{\mathcal{L}} = 1/\{1+[(\delta-\omega)T_2]^2\}$, where $\delta = \omega_g - \omega_c$ is the detuning of the gain peak from the frequency of the axial mode, and $1/T_2$ is its linewidth. $\Delta_\perp = \partial^2/\partial x^2 + \partial^2/\partial y^2$ is the transverse Laplacian describing diffraction, with $a$ the transverse spatial scale parameter. We define a "transverse frequency" of tilted waves by $\Omega_\perp = ak_\perp^2$. We will mainly use this $\Omega_\perp$ as a convenient measure of the transverse wave vector, avoiding the need for an explicit spatial scale.

Finally, in (1) the term $F$ describes the feedback effect. In integral form, it is given by

$$F(t) = \frac{\sigma}{2T}\int_{t-\tau-2T}^{t-\tau} dt' E(t') e^{i\omega_m(t-\tau-t')} \tag{2}$$

where $\sigma$ is the feedback strength, $\tau$ the delay time in the feedback loop, $\omega_m$ the detuning of the central maximum of the diffraction grating reflection from $\omega_c$, and $2T$ the time spread of the diffraction grating. The integral relation (2) can be transformed into a differential equation with delayed argument [14,19,25,26]:

$$\frac{dF}{dt} = \frac{\sigma}{2T}[E(t-\tau) - e^{2i\omega_m T}E(t-\tau-2T)] + i\omega_m F(t). \tag{3}$$

We use the differential description (3) for our numerical modeling.

As described above, the transmission through the FSF does not depend directly on wave number. Hence, spatial operators are not included in Eqs. (2) and (3).

## III. ANALYSIS

For any monochromatic field $E = E_0 e^{i\omega t}$, it follows from (2) or (3) that $F$ is proportional to $E$:

$$F = Re^{i\phi}E = \sigma\,\text{sinc}(\Delta)e^{-i(\omega\tau-\Delta)}E. \tag{4}$$

Here $\Delta = (\omega-\omega_m)T$, so the sinc term in (4) evidently describes the width and shape of the frequency selectivity of

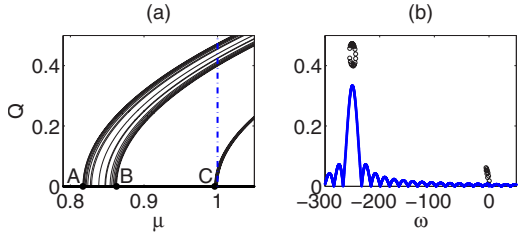


FIG. 2. (Color online) On-axis mode properties for flat gain spectrum. (a) The amplitudes $Q$ of the steady states versus pump current $\mu$. Points $A$, $B$, $C$ are described in the text. Parameters: $\sigma=60.0$, $\kappa=300.0$, $\alpha=5.0$, $\tau=5.0$, $T=0.1845$, $\omega_m=-250.0$. (b) Circles are the amplitudes $Q$ versus frequency for $\mu=1$ [vertical line in (a)]. Solid curve, relative amplitude of grating feedback function.

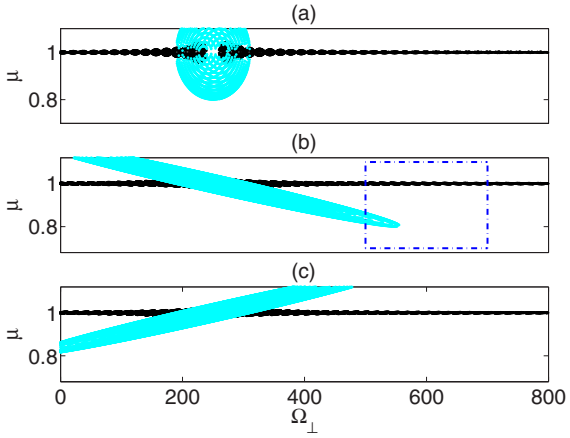


FIG. 3. (Color online) Thresholds of transverse modes in the $(\Omega_\perp,\mu)$ plane for different phase-amplitude couplings in the system with flat gain. (Every mode remains active for all current levels above its threshold.) $\omega_m=250.0$; other parameters as in Fig. 2. The gray (cyan) regions correspond to instabilities of the trivial solution determined mainly by FSF, the black to those determined mainly by the solitary VCSEL. $\alpha=$(a) 0.0; (b) 5.0 (the meaning of the rectangle is described in the caption of Fig. 4); (c) −5.0.

the grating feedback. Substitution of $F$ from (4) into (1) shows that the cavity loss rate $\kappa$ is modulated by the feedback, thus modulating the lasing threshold with a maximum range of $|\sigma\,\mathrm{sinc}(\Delta)|/\kappa$. The term $e^{-i\omega\tau}$ means that the relative phase of $F$ and $E$ is a rapidly varying function of frequency, ensuring that there are many lowered-threshold external-cavity modes under the main peak of the sinc function.

We now obtain monochromatic traveling-wave solutions, of the form $E=Qe^{i(\omega t-\mathbf{k}_\perp\cdot\mathbf{r}_\perp)}$, where we can assume $Q$ real and positive. These solutions can be referred to as steady states, because the time dependence is trivial: the absolute value of $E$ is constant and, since $E$ is an eigenstate of $\hat{\mathcal{L}}$, the corresponding value of $N$ is also constant.

In order to understand better the properties of the system, we consider first the case of flat gain, i.e., $T_2=0$ (and thus $\hat{\mathcal{L}}=1$). From Eqs. (1), (3), and (4) we can obtain equations for the frequencies and amplitudes of the traveling waves:

$$\omega-\Omega_\perp=R\sin(\phi)-\alpha R\cos(\phi), \tag{5}$$

$$Q^2=\frac{\kappa\mu}{\kappa-R\cos(\phi)}-1, \tag{6}$$

where $\Omega_\perp$ is the above-defined transverse frequency, and the magnitude $R$ and phase $\phi$ of $F/E$ are given by (4). Note that the dispersion relation (5) is wholly determined by external cavity parameters, and in particular is independent of the current $\mu$. Solutions to (5) are only physical for $Q^2$ positive, however, so that each has a threshold current at which the right side of (6) is zero. Since $R$ becomes small for frequencies well detuned from $\omega_m$, the threshold current for such modes is close to $\mu=1$, i.e., there is effectively no feedback. Modes close to $\omega_m$, in contrast, can have thresholds as low as $\mu=1-|\sigma|/\kappa$.

We first examine on-axis modes, for which $\Omega_\perp$ is zero. On-axis emission should be favored for negative $\omega_m$, and so we set $\omega_m=-250.0$. For this case, the dependence of the amplitude of on-axis modes on pump current $\mu$, for fixed values of the other parameters, is plotted in Fig. 2(a). We choose $\sigma=60$ and $\kappa=300$, so that lasing begins at $\mu\approx0.8$, well below the solitary laser threshold. At $A$ in Fig. 2(a) the first mode of a family with frequencies close to $\omega_m$ reaches threshold. The amplitudes of these modes then increase with current. At point $B$ the trivial solution becomes stable again, as the last mode of this grating-controlled family crosses the threshold. At the point $C$, a second mode family reaches threshold. These modes have frequencies close to zero [cf. Fig. 2(b)], and thresholds close to $\mu=1$, and so can be regarded as modes of the solitary VCSEL, with negligible feedback. It is clear from Fig. 2 that between points $B$ and $C$ we have a region where the trivial solution and on-axis external-cavity modes coexist.

We now consider modes with finite transverse wave vector, which corresponds to allowing finite (but necessarily positive) $\Omega_\perp$ in (5). For the moment we retain flat gain ($T_2=0$), so that the threshold of the solitary VCSEL is $\mu=1$ for every wave number and there is no internal pattern selection mechanism. Here we choose $\omega_m$ positive (=250.0) to favor off-axis modes.

For zero phase-amplitude coupling [Fig. 3(a)] the transverse frequencies with lowest thresholds are identical to the grating frequency, but a finite linewidth enhancement factor $\alpha$ shifts the minimum threshold away from $\Omega_\perp=\omega_m$ [e.g., $\alpha=5.0$, Fig. 3(b) and −5.0, Fig. 3(c)]. From (1) it is apparent that the longitudinal resonance of the VCSEL cavity shifts by $|\alpha\kappa|$ between $N=0$ and 1, and hence the threshold reduction due to feedback is accompanied by a frequency shift [14]. As a result, the oscillation frequency of any particular off-axis wave shifts with $N$, and hence with current. The cigar shapes in Figs. 3(b) and 3(c) essentially follow this shift, so as to maintain the grating resonance condition $\omega\approx\omega_m$.

It is apparent from Fig. 3 that, beyond the minimum threshold at $\mu\approx0.79$, the trivial solution is always unstable to some wave vector. Thus there is no bistability between off and on states of the laser (and hence there can be no localized lasing states). Note, however, that $R$, which determines the threshold envelope, is invariant if both $\omega_m$ and $\Omega_\perp$ are shifted by equal amounts. Thus, by appropriate choice of the grating frequency $\omega_m$, it may be possible to make all the troublesome transverse frequencies negative, and thus un-

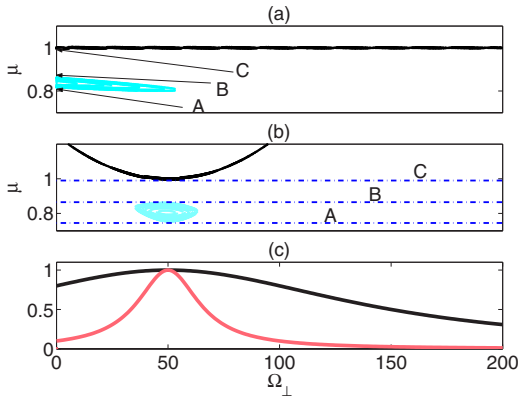


FIG. 4. (Color online) (a) Identical to the part of Fig. 3(b) enclosed by the rectangle, but shifted to the left because here $\omega_m=-250$. The points $A$, $B$, $C$ are identical to the equivalent points in Fig. 2(a). (b) Stability boundaries for system with spatially filtered feedback and finite gain bandwidth. The black line corresponds to solitary VCSEL modes, the light-gray (cyan) region to the modes controlled by FSF with spatial filtering. The trivial solution is unstable between lines $A$, $B$ and stable between lines $B$, $C$. (c) Dependence on transverse frequency of the relative feedback strength [gray (red) curve] and gain (black curve). Parameters as in (a) except for $\sigma=100.0$, $T_f=0.06$, $\delta_f=50.0$, $T_2=0.01$. The gain spectrum in (c) primarily affects the solitary VCSEL modes, for which it corresponds to $\delta=50.0$.

physical. This requires $\omega_m$ to be sufficiently negative, as in Fig. 4(a), which is identical to the dashed rectangle in Fig. 3(b). In Fig. 4(a) points $A$, $B$, $C$ are identical to the equivalent points in Fig. 2(a), and all tilted-wave mode thresholds lie below point $B$.

While the trivial solution is stable for current values in the range $(B,C)$, simulations show very complex dynamics in this region, and no stable localized states were found. To reduce the complexity, a spatial filter is introduced in the feedback equation, which works as a narrow-pass filter for a band of transverse frequencies (a ring in $k_\perp$ space)

$$\sigma(\Omega_\perp) = \frac{\sigma}{1+[(\delta_f-\Omega_\perp)T_f]^2}. \tag{7}$$

$\delta_f$ determines the band center of the filter and $T_f$ its width. Such a filter might be implemented experimentally by placing an annular aperture in the back focal plane of the first lens ($F$ in Fig. 1).

The filter should suppress all tilted waves outside its bandpass, while still allowing enough bandwidth to support tilted waves with slow spatial variations of their amplitudes (and, in particular, localized states). The traveling-wave solutions (5) and (6) remain valid for $\sigma(\Omega_\perp)$, and Fig. 4(b) depicts the same kind of information as Fig. 4(a), but with spatial filtering and a slightly higher feedback strength. The parameters were adjusted such that there is bistability between a stable trivial solution and off-axis modes in a substantial interval of pump current (between the lines $B$ and $C$), within which range localized states may exist.

In this figure, we have also included the effects of finite gain bandwidth [Fig. 4(b)]. In (1) the Lorentzian operator

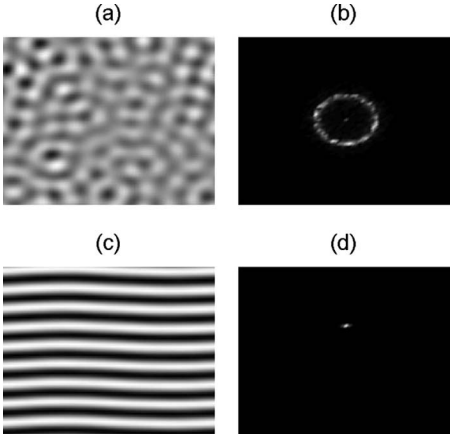


FIG. 5. Evolution of optical field $E$ for parameters of Fig. 4(b) and pump current $\mu=0.8$, for which $E=0$ is an unstable state. (a) Snapshot of the real part of the field during the transient stage; (b) far-field intensity during the transient stage; (c) snapshot of the real part of the field in the asymptotic regime; (d) far field in the asymptotic regime.

$\hat{\mathcal{L}}=1/\{1+[(\delta-\omega)T_2]^2\}$ describes the gain spectrum. It has been shown [16] that the output frequency of a broad-area VCSEL obeys $\omega=\omega_c+\Omega_\perp$, i.e., is selected by tilted-wave resonance [27,28]. We assume that similar slaving applies to our system, and thus that the gain spectrum can be considered a function of wave vector, rather than frequency, which is much more convenient for simulations. As expected, the minimum thresholds occur when the gain maximum coincides with the filter maximum, as in Fig. 4(c). The gain linewidth is set much smaller than in a real VCSEL, in order to show its main effect in this context, which is to warp the threshold curves in Fig. 4(b) for solitary VCSEL modes. In fact, even this unrealistically narrow gain bandwidth only weakly perturbs the strong frequency and wave vector selection imposed by the cavity, grating, and spatial filter.

## IV. SIMULATIONS

We have performed numerical simulations of the system of equations (1) and (3) using a split-step Runge-Kutta method with fixed step size. Polynomial interpolation was used to calculate the value of the field at intermediate times inside the delay interval. The spatial operators were evaluated in Fourier space. The calculations were performed using a cluster of parallel processors with large shared-access memory because of the need to store all the spatial data throughout the delay interval.

For values of the pump current within the dark-gray (red) region in Fig. 4(a), modes with wave numbers in the passband emerge from noise, leading to a ring in the far field and irregular structures in the near field [Figs. 5(a) and 5(b)]. The radius of the far-field ring corresponds to $k_f=\sqrt{\delta_f/a}$ as expected. After this transient stage, however, the field evolves through winner-take-all mode competition toward a single traveling wave [Figs. 5(c) and 5(d)], as expected for an infinitely extended laser [29]. In this case, the field amplitude is homogeneous, but its real part shows stripes and there is a

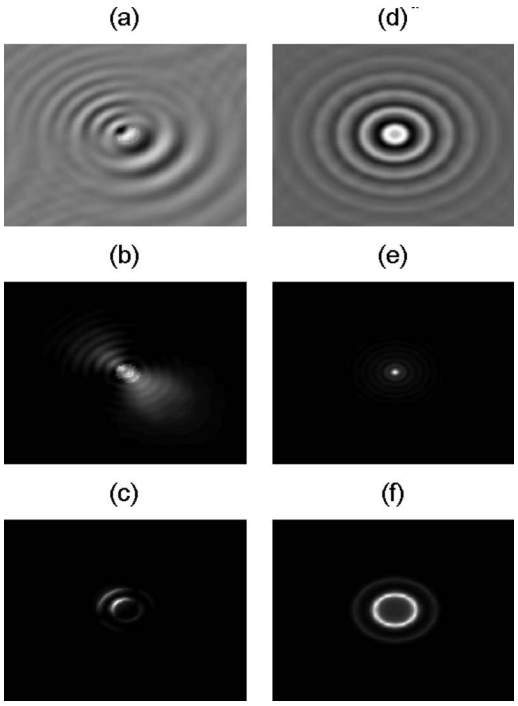


FIG. 6. Snapshots of localized lasing states for the same parameters as in Fig. 5, except $\mu=0.9$, for which $E=0$ is stable. (a), (d) are the real part of the field, (b), (e) are the intensities of the field ($|E|^2$), and (c), (f) are the far-field intensity distributions. (a), (b), (c) correspond to a localized traveling wave, (d), (e), (f) correspond to a localized standing wave (LSW). The different structures are excited using different initial conditions; see text.

single spot in the far field which lies on the ring of unstable modes [see Fig. 5(b)]. Increasing the pump current into the range where the trivial solution regains stability [above line $B$ but below $C$ in Fig. 4(a)], the traveling wave (TW) remains stable. Hence there is coexistence between an extended, spatially nontrivial solution (here the TW) and the trivial solution, which is known to provide favorable conditions for localized structures [2,30].

In order to excite a localized structure, the system is initialized with the trivial solution, except for a disk in the center of the transverse section, which is initialized with the coexistent TW. A stable localized structure evolves, which looks like part of a TW [Figs. 6(a)–6(c)]. In particular the far field [Fig. 6(c)] is off center and asymmetric, so we term this a localized traveling wave. The amplitude $|E(x,y)|$ of the field is constant in time, while the real part performs regular oscillations (at any fixed point) with a frequency close to $\omega_m$. The stationary envelope of the LTW overlies a traveling wave which propagates through it with phase velocity $\approx\omega_m/k_f$. It is interesting to note that similar LTW structures have been found in hydrodynamical systems [31,32].

Detailed numerical analysis of LTW structures confirms that they possess key properties expected of dissipative self-localized solutions, i.e., cavity solitons. First, the intensity decays almost exponentially from the central maximum toward the zero background (Fig. 7). This also implies exponential decay of $r|E|^2$ as $r\to\infty$, in contrast with Bessel beams, for which this quantity, essentially the energy per

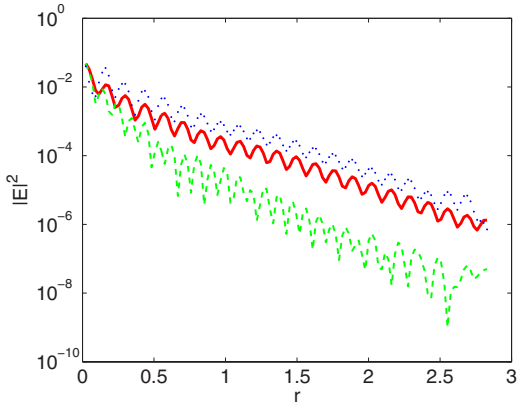


FIG. 7. (Color online) Evidence of the self-localization of the LTW state. Displayed is the intensity $|E|^2$ of the field versus the distance $r$ from its peak. Note the logarithmic intensity scale, so that the linear decrease of each of three intensity measures shows exponential localization. Solid curve is the azimuthally averaged intensity. Dotted and dashed curves are two orthogonal sections. These curves are calculated over a radial range four times larger than that displayed in Fig. 6.

annulus, remains constant. Second, the structure can be present or absent for the same parameters. Third, the LTW can be excited in any region of the transverse section, i.e., has freedom of location. Fourth, it is an attractor of the dynamics, forming and stabilizing from nonsmooth initial conditions only approximating the amplitude and width of the LTW. We have also found similar LTW structures for other parameter values. In particular, they exist also for flat gain ($T_2=0$), and so are not sensitive to the particular width or shape of the gain spectrum.

We can also excite a different sort of localized structure with initial conditions consisting of a radially symmetric (Gaussian) pulse. The frequency of this address pulse is that of the external cavity mode of maximal amplitude, and its duration is equal to the delay time $\tau+2T$. A symmetric stable localized structure is created [Figs. 6(d)–6(f)], which we term a localized standing wave (LSW). In the real part, the center oscillates with constant frequency, while the tail is like an inward-traveling wave. The intensity at any point is constant.

As well as the self-focusing case $\alpha=5.0$ described above, we have checked the self-defocusing case $\alpha=-5.0$, for which the stability boundaries of the trivial solution are depicted in Fig. 3(c). However, by appropriate choice of $\omega_m$ and the spatial filter parameters, it is again possible to obtain bistability, and LTWs can be excited in the same way. Hence self-localization does not depend on the sign of the phase-amplitude coupling.

The mutual independence of these self-localized structures is demonstrated explicitly in Fig. 8 where it is shown that several, of different types, can stably coexist within the transverse plane (Fig. 8).

## V. CONCLUSIONS

In summary, we have presented and analyzed a model of a VCSEL with frequency-selective external feedback, and

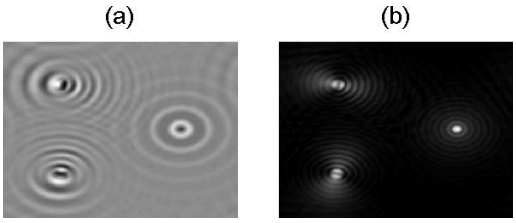


FIG. 8. Stable coexistence of several localized structures, two LTWs with different orientations (on the left) and one LSW. Image area is four times larger than in Fig. 6. (a) Real part and (b) amplitude of field.

shown that the system supports traveling-wave solutions. More significantly, we have found conditions under which the traveling waves can coexist with the trivial laser off state. We showed stable coexistence of a single transverse traveling wave with a homogeneous solution with spatially filtered feedback. Such coexistence often implies the existence of localized solutions, and indeed we have presented numerical evidence for the occurrence of such solutions in our system. These self-localized traveling and standing waves satisfy all of the important criteria for conventional cavity solitons: exponential localization, presence or absence under the same conditions, and freedom of location.

These results have several interesting aspects. In the first place, they pave the way for realizing a semiconductor-based cavity soliton laser using fairly standard designs. Second, we have demonstrated localized structures (LTWs and LSWs) which, because of their unusual internal structures (and, in the case of the LTWs, spatial asymmetry), are quite different in nature from the well-established cavity solitons mentioned in the Introduction. They do have particlelike properties, however, similar to those of other dissipative solitons, and so we claim that our model does indeed describe a cavity soliton laser. The interactions of these LTW and LSW solitons with each other and with external "forces" is an important area for future investigation—Fig. 8 already shows that the interaction has a limited range. Other studies on cavity solitons show an oscillatory interaction at short distances, leading to bound states (e.g., [5,8,33]), and some recent results indicate intricate features of the interaction of asymmetric solitons [34]. Third, semiconductor lasers with optical feedback are known to show a wide variety of temporal instabilities, and preliminary results indicate that the system under study is no exception. Studying the properties of regularly and irregularly oscillating localized structures may be fruitful for fundamental insights into spatiotemporal dynamics and chaos, and possible synchronization (within the same device or in coupled devices) has potential for chaotic data transmission [35].

## ACKNOWLEDGMENTS

P.V.P. was supported by INTAS Grant No. 04-83-3276. The work of A.J.S., T.A., and W.J.F. was carried out in the framework of EU-STREP Grant No. 4868 FunFACS. We are grateful to R. Martin for help and for the efficient operation of the parallel processor cluster.

[1] P. Coullet, Int. J. Bifurcation Chaos Appl. Sci. Eng. **12**, 2445 (2002).
[2] *Dissipative Solitons*, edited by N. Akhmediev and A. Ankiewicz (Springer, New York, 2005).
[3] M. Brambilla, L. A. Lugiato, F. Prati, L. Spinelli, and W. J. Firth, Phys. Rev. Lett. **79**, 2042 (1997).
[4] V. B. Taranenko, K. Staliunas, and C. O. Weiss, Phys. Rev. A **56**, 1582 (1997).
[5] B. Schäpers, M. Feldmann, T. Ackemann, and W. Lange, Phys. Rev. Lett. **85**, 748 (2000).
[6] N. N. Rosanov, *Spatial Hysteresis and Optical Patterns*, Springer Series in Synergetics (Springer, Berlin, 2002).
[7] S. Barland *et al.*, Nature (London) **419**, 699 (2002).
[8] P. L. Ramazza, E. Benkler, U. Bortolozzo, S. Boccaletti, S. Ducci, and F. T. Arecchi, Phys. Rev. E **65**, 066204 (2002).
[9] L. A. Lugiato, IEEE J. Quantum Electron. **39**, 193 (2003).
[10] M. Pesch, E. Grosse Westhoff, T. Ackemann, and W. Lange, Phys. Rev. Lett. **95**, 143906 (2005).
[11] V. B. Taranenko and C. O. Weiss, Appl. Phys. B: Lasers Opt. **72**, 893 (2001).
[12] S. Barbay, Y. Ménesguen, X. Hachair, L. Leroy, I. Sagnes, and R. Kuszelewicz, Opt. Lett. **31**, 1504 (2006).
[13] http://www.funfacs.org
[14] A. Naumenko, N. Loiko, M. Sondermann, K. Jentsch, and T. Ackemann, Opt. Commun. **259**, 823 (2006).
[15] Y. Tanguy, T. Ackemann, and R. Jäger, Phys. Rev. A **74**, 053824 (2006).
[16] M. Schulz-Ruthenberg *et al.*, Appl. Phys. B: Lasers Opt. **81**, 945 (2005).
[17] M. Bache, F. Prati, G. Tissoni, R. Kheradmand, L. A. Lugiato, I. Protsenko, and M. Brambilla, Appl. Phys. B: Lasers Opt. **81**, 913 (2005).
[18] Y. Tanguy, M. Schulz-Ruthenberg, and T. Ackemann (unpublished).
[19] M. Yousefi and D. Lenstra, IEEE J. Quantum Electron. **35**, 970 (1999).
[20] I. V. Babushkin, N. A. Loiko, and T. Ackemann, Phys. Rev. E **69**, 066205 (2004).
[21] N. A. Loiko and I. V. Babushkin, J. Opt. B: Quantum Semiclassical Opt. **3**, S234 (2001).
[22] T. Rossler, R. A. Indik, G. K. Harkness, J. V. Moloney, and C. Z. Ning, Phys. Rev. A **58**, 3279 (1998).
[23] C. Degen, I. Fischer, W. Elsasser, L. Fratta, P. Debernardi, G. Bava, M. Brunner, R. Hovel, M. Moser, and K. Gulden, Phys. Rev. A **63**, 023817 (2001).
[24] J. Martin-Regalado, F. Prati, M. San Miguel, and N. B. Abraham, IEEE J. Quantum Electron. **33**, 765 (1997).
[25] A. P. A. Fisher, O. K. Andersen, M. Yousefi, S. Stolte, and D. Lenstra, IEEE J. Quantum Electron. **36**, 375 (2000).
[26] M. Guidici, L. Giuggioli, C. Green, and J. R. Tredicce, Chaos,

Solitons Fractals **10**, 811 (1999).
[27] P. K. Jakobsen, J. V. Moloney, A. C. Newell, and R. Indik, Phys. Rev. A **45**, 8129 (1992).
[28] A. C. Newell and J. V. Moloney, *Nonlinear Optics* (Addison Wesley, Redwood City, CA, 1992).
[29] G. K. Harkness, W. J. Firth, J. B. Geddes, J. V. Moloney, and E. M. Wright, Phys. Rev. A **50**, 4310 (1994).
[30] P. Coullet, C. Riera, and C. Tresser, Phys. Rev. Lett. **84**, 3069 (2000).
[31] J. J. Niemela, G. Ahlers, and D. S. Cannell, Phys. Rev. Lett. **64**, 1365 (1990).
[32] K. Lerman, E. Bodenschatz, D. S. Cannell, and G. Ahlers, Phys. Rev. Lett. **70**, 3572 (1993).
[33] A. G. Vladimirov, J. M. McSloy, D. V. Skryabin, and W. J. Firth, Phys. Rev. E **65**, 046606 (2002).
[34] N. N. Rosanov, S. V. Fedorov, and A. N. Shatsev, Phys. Rev. Lett. **95**, 053903 (2005).
[35] A. Argyris, D. Syvridis, L. Larger, V. Annovazzi-Lodi, P. Colet, I. Fischer, J. Garcia-Ojalvo, C. R. Mirasso, L. Pesquera, and A. Shore, Nature (London) **437**, 343 (2005).